Supplementary Material for

***Doping and Defect Co-Engineering Strategy to Overcome Gain-Speed Dilemma of $Ga_2O_3$ Thin Film Grown by Mist-CVD Technique***

**Supplementary information S1: The raw data of XRD result.**

The raw data of XRD result is shown in **Fig. S1**. In all samples, only peaks at around 40.20° can be found, which belong to $\alpha$-$Ga_2O_3$ (0006), and there are no peaks found at 39.02° and 38.9°, which belong to$\varepsilon$-$Ga_2O_3$ (004) and $\beta$-$Ga_2O_3$ (-201), respectively.

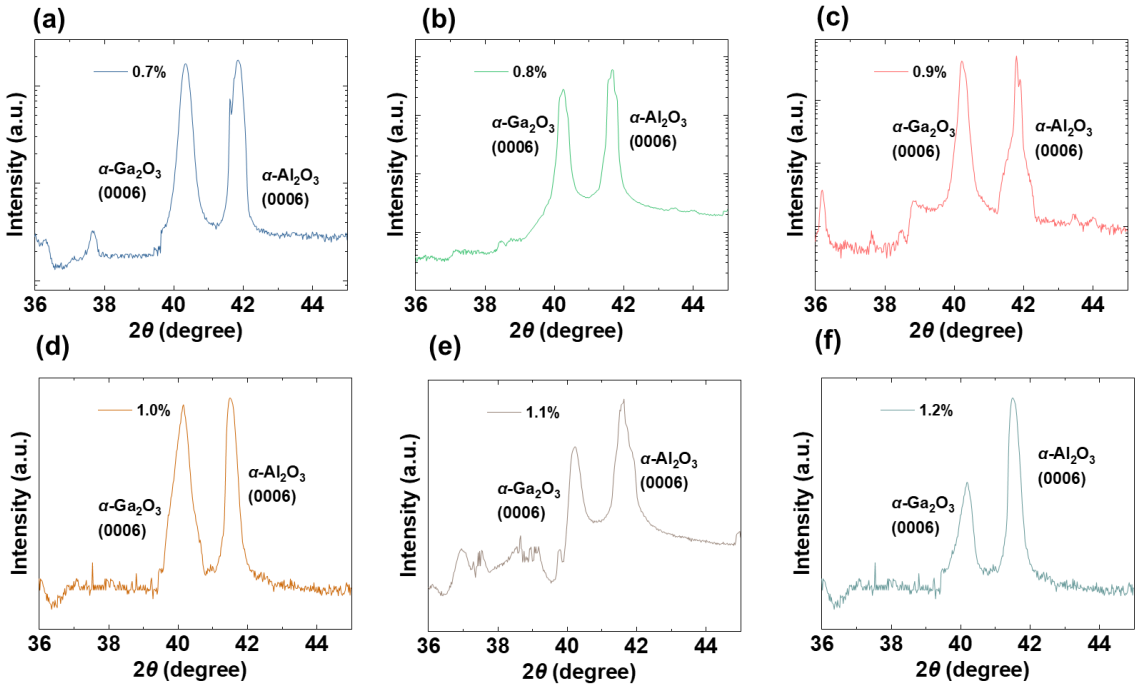


**Fig. S1**. The raw XRD result of thin film from precursor with acid of (a) S1, (b) S2, (c) S3, (d) S4, (e) S5, (f) S6.

**Supplementary information S2: X-ray diffraction rocking curve.**

To further evaluate the crystalline quality of the Sn-doped $\alpha$-$Ga_2O_3$ films, we performed X-ray rocking curve (XRC) measurements. As shown in **Fig. S2**, the full width at half maximum (FWHM) of the $\alpha$-$Ga_2O_3$ (0006) rocking curve was less than 300 arcsec for all samples, indicating reasonably good crystalline quality. However, the FWHM values were generally higher than those reported in the literature and observed in our own unintentionally doped (UID) $\alpha$-$Ga_2O_3$ films, supporting the assessment that the crystalline quality, while acceptable, was not ideal. Notably, samples S3, S4, and S5 exhibited lower FWHM values (less than 150 arcsec) compared to the other Sn-doped samples, suggesting superior crystalline quality. This trend correlates with their higher peak intensities observed in the $2\vartheta$ scans, confirming a relationship between peak intensity and crystalline quality.

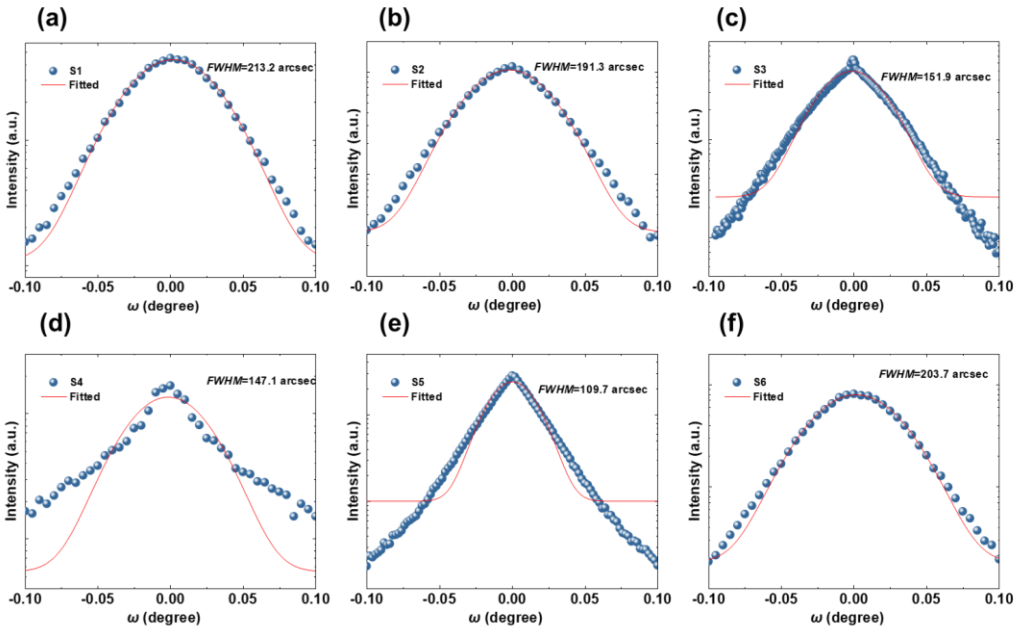


**Fig. S2** XRD rocking curve of α-$Ga_2O_3$ (0006) peak of sample (a) S1, (b) S2, (c) S3, (d) S4, (e) S5, (f) S6.

**Supplementary information S3: The optical absorption of samples.**

The UV-vis absorbance spectrums of the all samples are shown in **Fig. S3**. Considering UID $\alpha$-$Ga_2O_3$ as a direct band gap semiconductor, the optical band gap of $\alpha$-$Ga_2O_3$ can be evaluated by Tauc's formula: $(\alpha h\nu)^2=C(h\nu-E_g)$, where $\alpha$ is the absorbance coefficient, C is a constant, h is Planck's constant and $\nu$ is the incident light frequency. As shown in the inset of **Fig. S3** The optical bandgap of samples are confirmed by extrapolating the linear region of Tauc plot.

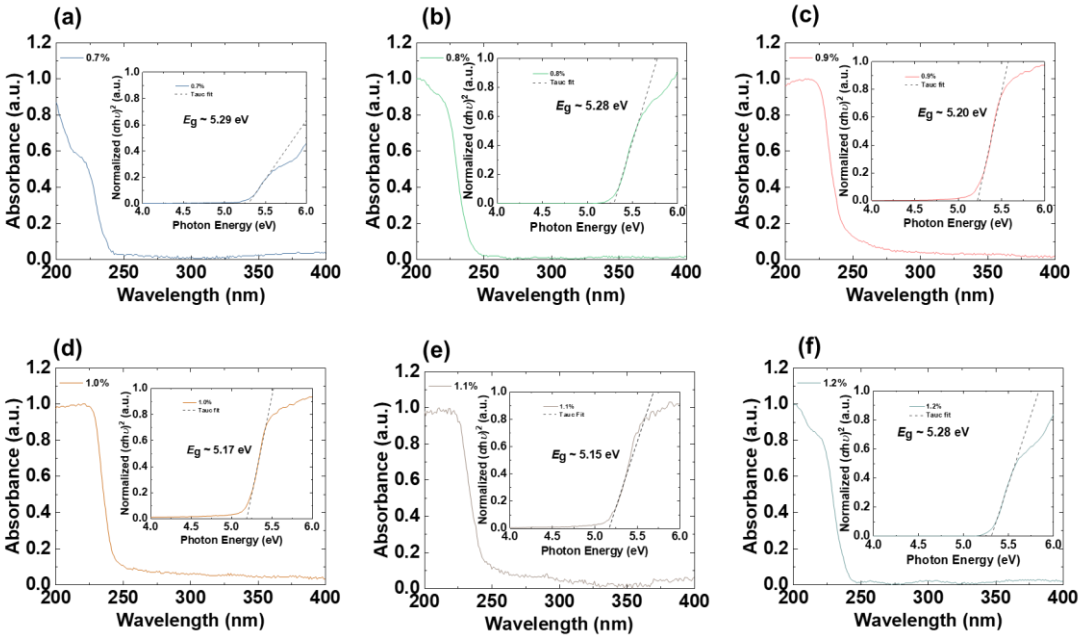


**Fig. S3**. Raw data of absorption spectrum and Tauc plot of (a) S1, (b) S2, (c) S3, (d) S4, (e) S5, (f) S6.

**Supplementary information S4: Photoresponse Characteristics of samples.**

The photoresponse characteristics are shown in **Fig.** S4. In **Fig.** S4(a), where dark current ($I_d$) and photo current ($I_{ph}$) are measured under 10 V, and the incident light intensity is of 412.2 μW/cm$^2$.

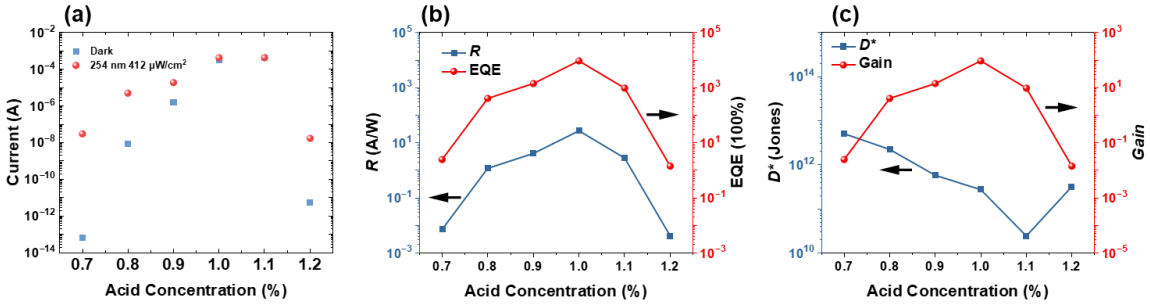


**Fig. S4**, (a) dark current and photo current, (b) R and EQE, (c) D* and photoconductor gain of the deposited films.

Meanwhile, key parameters for evaluating the photoresponse characteristics are calculated and shown in **Fig. S4**(b) and (c), which include responsivity ($R$), external quantum efficiency (EQE), specific detectivity ($D^*$), and photoconductive gain ($G$). which are calculated based on following formula[1,2],[3,4,5]:

$$R = \frac{I_{ph} - I_d}{AS} \tag{1}$$

$$\boldsymbol{EQE = \frac{hcR}{e\lambda}} \tag{2}$$

$$D^* = \frac{\sqrt{A_\Delta f}}{NEP} = R\sqrt{\frac{A}{2eI_d}} \tag{3}$$

$$\boldsymbol{G = \frac{\tau}{T_r} = \frac{EQE}{IQE}} \tag{4}$$

If IQE=1

$$\boldsymbol{G \equiv EQE = \frac{\Delta Q/e}{\frac{\Delta_{E_{ph}}}{h\nu}} = \frac{(I_{ph} - I_d)/e}{AP/h\nu}} \tag{5}$$

Where $A$ is the efficient irradiated area which is considered as 0.01 cm$^2$ in this study, $P$ is the light intensity, h is Planck's constant, c is the light velocity, e is the electronic charge, $\lambda$ is the wavelength of incident light, $\Delta f$ is the bandwidth, $NEP$ the noise equivalent power, $\tau$ is carrier lifetime and $T_r$ is the transit time of a carrier between electrodes. It should be noted that $G$ is the ratio of EQE to internal quantum efficiency (IQE), and For $Ga_2O_3$ materials, the absorption coefficient α in the UVC

region (especially near 254 nm) is typically larger than $10^5$ $cm^{-1}$. According to the Beer-Lambert law, a film thickness of approximately 400 nm (samples in this study are all around 500 nm) is sufficient to absorb over 99% of the incident solar-blind photons.

It should be noted that, due to the practical limitations of our current characterization equipment and testing conditions, only the shot noise was taken into accounts when calculating the specific detectivity ($D^*$), while according to this consensus[6], the potential contributions from other noise sources (such as flicker noise and thermal noise) were not included. Consequently, the $D^*$ values reported herein might be systematically overestimated compared to the actual absolute values. Nevertheless, because an identical calculation formulation and protocol were consistently applied across all samples under identical configurations, the relative trend and comparison of $D^*$ among the different experimental groups studied in this work remain highly valid and physically meaningful.

**Supplementary information S5: Full XPS Spectra**

The origin data of full spectrum XPS result was shown in **Fig. S5**, where the binding energies of Ga $2p_{1/2}$, Ga $2p_{3/2}$, Sn 3d, and O 1s are1144.91 eV 1118.07 eV, 485.77 eV, and 530.5 eV, respectively.

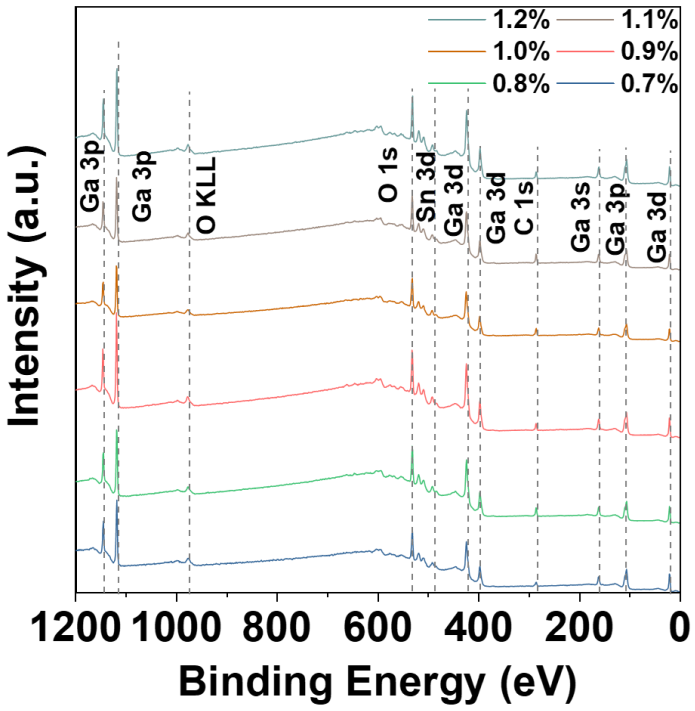


**Fig. S5**, the origin data of the full XPS spectrum.

**Supplementary information S6: High resolution XPS spectrum of Sn 3d.**

Sn $3d_{5/2}$ can be fitted into two components: $Sn^{2+}$ (peak at 485.9 eV) and $Sn^{4+}$ (peak at 486.6 eV) as shown in **Fig. S5**[7]. Also Sn $3d_{3/2}$ can be fitted into two components: $Sn^{2+}$ (peak at 492.8 eV) and $Sn^{4+}$ (peak at 494.6 eV) as shown in **Fig. S6**[8]. Comparison between two fitted result was illustrated in **Fig. S7**, and there is minor difference between Sn valance distribution extracted from Sn $3d_{5/2}$ and Sn $3d_{3/2}$.

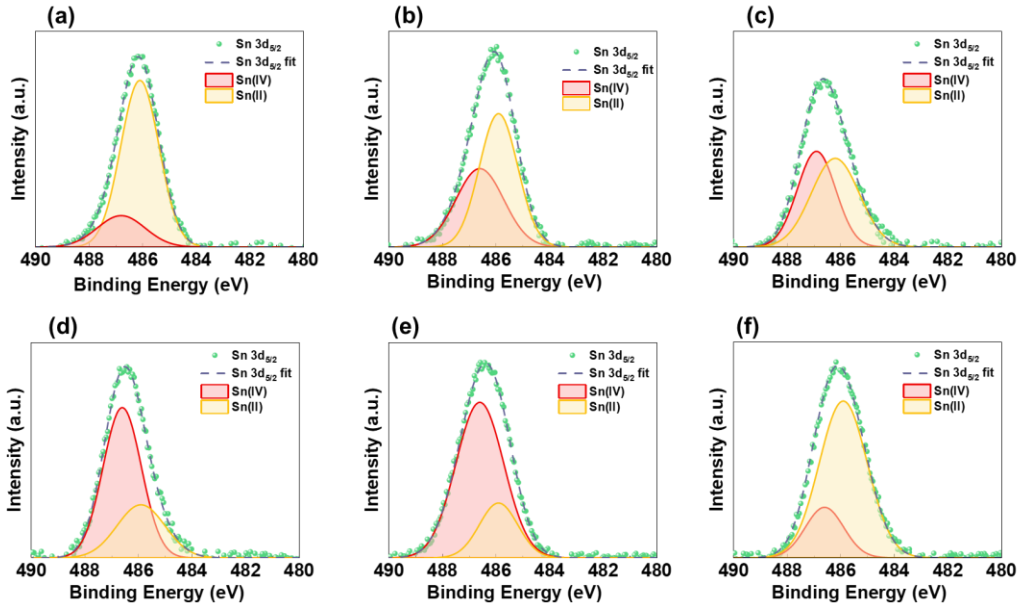


**Fig. S6** The high-resolution XPS spectrum of the Sn $3d_{5/2}$ for samples from precursor with acid concentration of (a) S1, (b) S2, (c) S3, (d) S4, (e) S5, (f) S6.

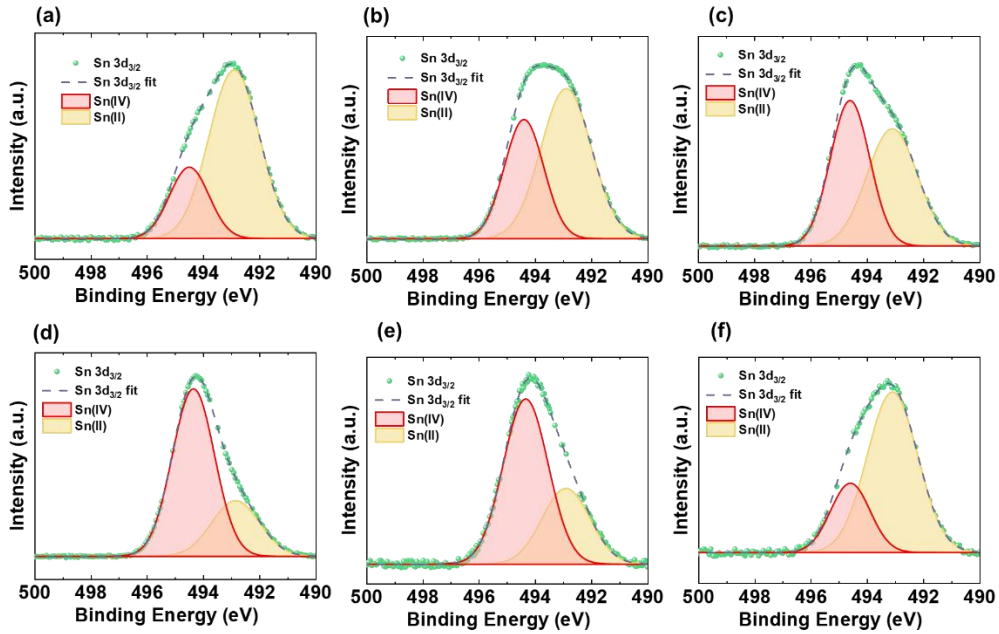


**Fig. S7** The high-resolution XPS spectrum of the Sn $3d_{3/2}$ for samples from precursor with acid concentration of (a) S1, (b) S2, (c) S3, (d) S4, (e) S5, (f) S6.

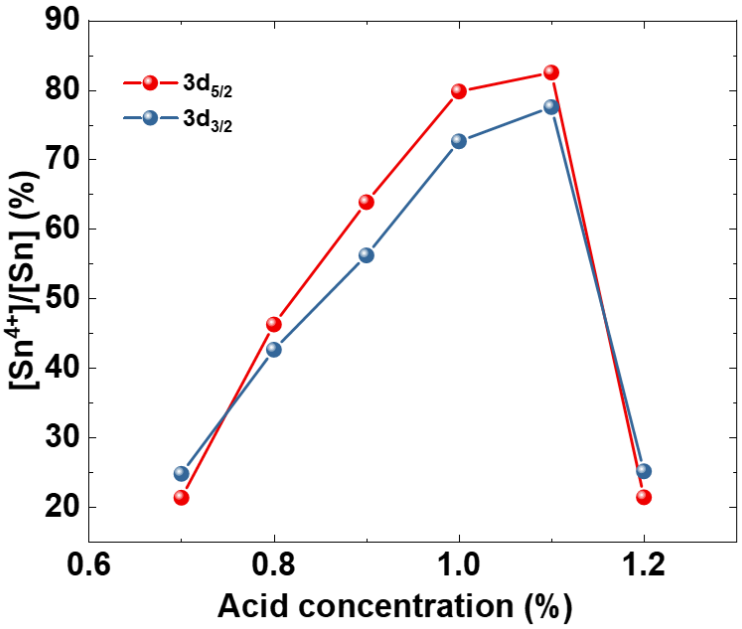


**Fig. S8** atomic ratio of $[Sn^{4+}]/[Sn]$ extracting from Sn $3d_{3/2}$ and $3d_{5/2}$.

## Reference


1 X. Gong, M. Tong, Y. Xia, W. Cai, J. S. Moon, Y. Cao, G. Yu, C.-L. Shieh, B. Nilsson and A. J. Heeger, *Science*, 2009, **325**, 1665–1667.

2 E. Monroy, F. Omns and F. Calle, *Semicond. Sci. Technol.*, 2003, **18**, R33–R51.

3 C. Soci, A. Zhang, X.-Y. Bao, H. Kim, Y. Lo and D. Wang, *j nanosci nanotechnol*, 2010, **10**, 1430–1449.

4 A. Rose, *Proc. IRE*, 1955, **43**, 1850–1869.

5 J. A. Garrido, E. Monroy, I. Izpura and E. Muñoz, *Semicond. Sci. Technol.*, 1998, **13**, 563–568.

6 V. Pecunia, T. D. Anthopoulos, A. Armin, B. Bouthinon, M. Caironi, A. Castellanos-Gomez, Y. Chen, K. Cho, C. Clegg, X. Fang, P. Fendel, B. Fowler, G. Gelinck, H. Gottlob, P. Guyot-Sionnest, R. Hannebauer, G. Hernandez-Sosa, M. C. Hersam, L. Hirsch, J. C. Ho, F. H. Isikgor, J. Joimel, H. J. Kim, G. Konstantatos, J. Labram, M. C. Lemme, K. Leo, E. Lhuillier, E. Lidorikis, M. A. Loi, P. E. Malinowski, P. Merken, T. Mueller, B. Nasrollahi, D. Natali, T. N. Ng, T.-Q. Nguyen, S. K. Park, L.-M. Peng, P. Samorì, E. H. Sargent, L. Shen, S. Shishido, I. Shorubalko, P. Sonar, S. D. Stranks, S. F. Tedde, K. Vandewal, M. Verhaegen, S. Walia, F. Yan, T. Yokota and F. Zhang, *Nat. Photon.*, 2025, **19**, 1178–1188.

7 M. Kwoka, L. Ottaviano, M. Passacantando, S. Santucci, G. Czempik and J. Szuber, *Thin Solid Films*, 2005, **490**, 36–42.

8 S. C. Su, H. Y. Zhang, L. Z. Zhao, M. He and C. C. Ling, *J. Phys. D: Appl. Phys.*, 2014, **47**, 215102.